Military Technical College
Kobry El-Kobba
Cairo, Egypt

12-th International Conference
on
Aerospace Sciences &
Aviation Technology

EFFECTS OF AIR AND FUEL FLOW ON THE DYNAMIC PERFORMANCE FOR A TURBOSHAFT GAS TURBINE ENGINE

PART I: MODELING AND SIMULATION

M. Metwally*, I. Saleh **, M.G.Rabie*** N. Girgis ****

Abstract

The dynamic performance of a turboshaft gas turbine engine is investigated in this paper. The air flows inlet to the engine and to the power turbine, are controlled by means of two guide vanes cascade. The displacement of the inlet guide vanes is controlled by means of two electrohydraulic servo actuators. The fuel flow rate is controlled by another electrohydraulic controller incorporating a series pressure compensated flow control valve. The equation describing the basic system subsystems and controllers were deduced and applied to develop a simulation program. The simulation program of the electrohydraulic servo controllers was validated experimentally. The engine dynamic performance is studied theoretically using the developed computer simulation program. Simulated results are shown for the transient response of the engine air and fuel flow control systems and its effect on the engine performance. The simulation results of engine air flow control show an agreement with the validated experimental results.

Key Words

Gas turbine engine, Engine control, Electrohydraulic, Proportional, Electromagnetic, Solenoid, Valve, and Actuator.

* Ph. D. Applicant, Egyptian Armored Force.
** Professor, Military Technical Collage
*** Professor, Modern Academy for Engineering and Technology
****Assoc. Professor, Military Technical Collage.

Nomenclatures

A	Cross section area, m^2
B	Bulk's modules, Pa
b	Perimeter, m.
C	Absolute velocity, m/s
C_d	Discharge coefficient.
C_h	Friction loss coefficient, N.s/m.
c	Specific heat, J/kg.^{o}K.
D	Diameter, m.
E	Energy, J.
e	Specific energy, J/kg.
F	Force; N.
f	Friction coefficient; N s/m.
G	Torque, N m.
g	The gravitational acceleration, m/s^2.
H_u	Fuel heating value, kJ s/kg.
h	Specific enthalpy, J/kg ^{o}K.
i	Current, A
j	Polar moment of inertia, kg m^2.
K	Spring stiffness; N/m
k_b	Feed back gain, A/m
L	Length, m.
M	Mach number.
m	Mass, kg.
$\dot{m}$	mass flow rate, kg/s.
N	Number of compressor stage.
n	Speed, r.p.s.
P	Power, W.
p	Total pressure, Pa.
Q	Pump flow rate, m^3/s
q	Heat added to the combustion chamber, kJ
R	Universal gas constant, J/mol ^{o}K, m or
R_L	Pump resistance.
r	Radius, m.
U	Compressor rotor wheel speed, m/s
V	Volume, m^3
v	Velocity, m/s.
W	Work, J or relative velocity, m/s.
x	Displacement, m.
z	Height, m.
α	Absolute velocity angle , deg.
	Relative velocity angle , deg.
	Air specific heat ratio.
	Efficiency.
	Compressor stage reaction coefficient.
	Viscosity coefficient, N s/m^2.
	Pressure ratio.

- □ Pressurizing valve spool inclination angle, deg.
- ρ Fluid density, kg/m^3.
- □ Coefficient of conservation of total pressure or Slip factor.
- □ Angular velocity, rad/s.

Subscript

1	Supply.	p	Pressure or valve piston.
1i	Valve down steam.	pc	Pressure compensated.
2	Regulated.	pr	Pressurized valve.
3	Reference.	R	Valve regulator
a	Engine intake air.	rc	Spool radial clearance.
A	Piston cap side.	rv	Relief valve.
B	Piston rod side.	s	Valve spool.
c	Solenoid core.	seat	Valve seat.
f	Fuel or Friction loss.	spc	Pressure compensator spool.
i	Internal leakage.	st	Short tube.
g	Gases or geometric volume.	t	Turbulent.
lm	Fuel pump losses.	th	Throttle or thermal.
M	Magnetic.	u	The tangential component.
m	Metering valve or mechanical.	v	Pressure amplifier chamber.
o	Valve return or stagnation.	x	Metering pressure amplifier.

Abbreviations

AGB	Accessory gear box	IGV	Inlet guide vane
CC	Combustion chamber	LPC	Low pressure compressor
DPRV	Deferential pressure regulator valve	LPT	Low pressure turbine
ECU	Electronic control unit	LVDT	Linear variable deferential transformer
EHSA	Electrohydraulic servo actuator		
FCU	Fuel control unit	PT	Power turbine
FMU	Fuel metering unit	PTS	Power turbine stator
HPC	High pressure compressor	RC	Recuperator
HPT	High pressure turbine	RGB	Reduction gear box

1. Introduction

The gas turbine engines suffer transient operation during the startup, shutdown, load changes, and abnormal emergency operation. During the transient operation, the system response should be as short as possible and temporal peaks of main parameter such as turbine inlet temperature and component rotational speed should not exceed certain reference values required for safe and reliable operation. Therefore, a precise prediction of the dynamic response of gas turbine engines is very important for stable operation, fault diagnosis, controller design, etc. To study the effect of air and fuel flow control on the dynamic performance of the gas turbine engine, the engine as a controlled system must be analyzed statically and dynamically.

The study starts by deducing a mathematical model describing the engine operation. The deduced mathematical model consists of a set of non linear differential and algebraic equations. These equations are obtained by the application of several laws

used to describe the physical phenomena such as dynamical motion, thermodynamic behavior….etc.
The analytical and experimental investigations of the transient behavior of gas turbine engine began around 1950[s]. Several mathematical models and methods for predicting the transient behavior have been proposed and applied to analyze system dynamic characteristics.
On 1983, Rowen [1] presented a simplified mathematical representation of a gas turbine engine. The engine is represented by a first order transfer function. He presented an analysis of a frequency response and a design of a speed control. On 1998, Corsa [2] presented a Simulink program for the aero-thermodynamic simulation of a gas turbine engine and investigated its transient response. On 2001, Kim [3] presented an investigation of a transient performance of a gas turbine engine based on a one-dimensional conservation equation. He presented also a modified dynamic simulation of full startup procedure of heavy duty gas turbine engine [4].
A contactless controlled spool electrohydraulic proportional actuator is employed to control the air and gases flow through the studied engine. Dynamic simulations of the air and gases flow control through the studied engine have been investigated theoretically and experimentally [5].
Herein, in part 1, a mathematical model and simulation program were developed to study the effect of air and fuel flow on the dynamic performance of a land system gas turbine engine. The governing equations were deduced and used to simulate the dynamic performance of the engine.

2. Gas turbine engine under study

The engine under study is a turboshaft gas turbine engine of 1500 hp (1118.5 kW) output shaft power, Fig. (1). It is a free-power turbine engine that utilizes a two-spool compressor and a counter flow type stationary heat exchanger (recuperator). The studied gas turbine engine consists of:
Inlet guide vane (IGV).
Low pressure compressor (LPC); a 5-stage axial flow compressor.
High pressure compressor (HPC); a 4-stage axial flow compressor and a single stage radial flow compressor.
Combustion chamber (CC); single can type.
High pressure turbine (HPT); single stage axial flow turbine.
Low pressure turbine (LPT); single stage axial flow turbine.
Power turbine (PT); a two-stage axial flow turbine.
Recuperator (RC).
Accessory gearbox (AGB); drive the engine fuel flow control unit (FCU).
Reduction gearbox (RGB); reduce the PT speed.

3. Mathematical model of the studied engine

The basic equations are used to model the parts performance of the studied gas turbine engine. The equations are written for different parts of the engine to predict the overall engine dynamic performance, [1] and [5].

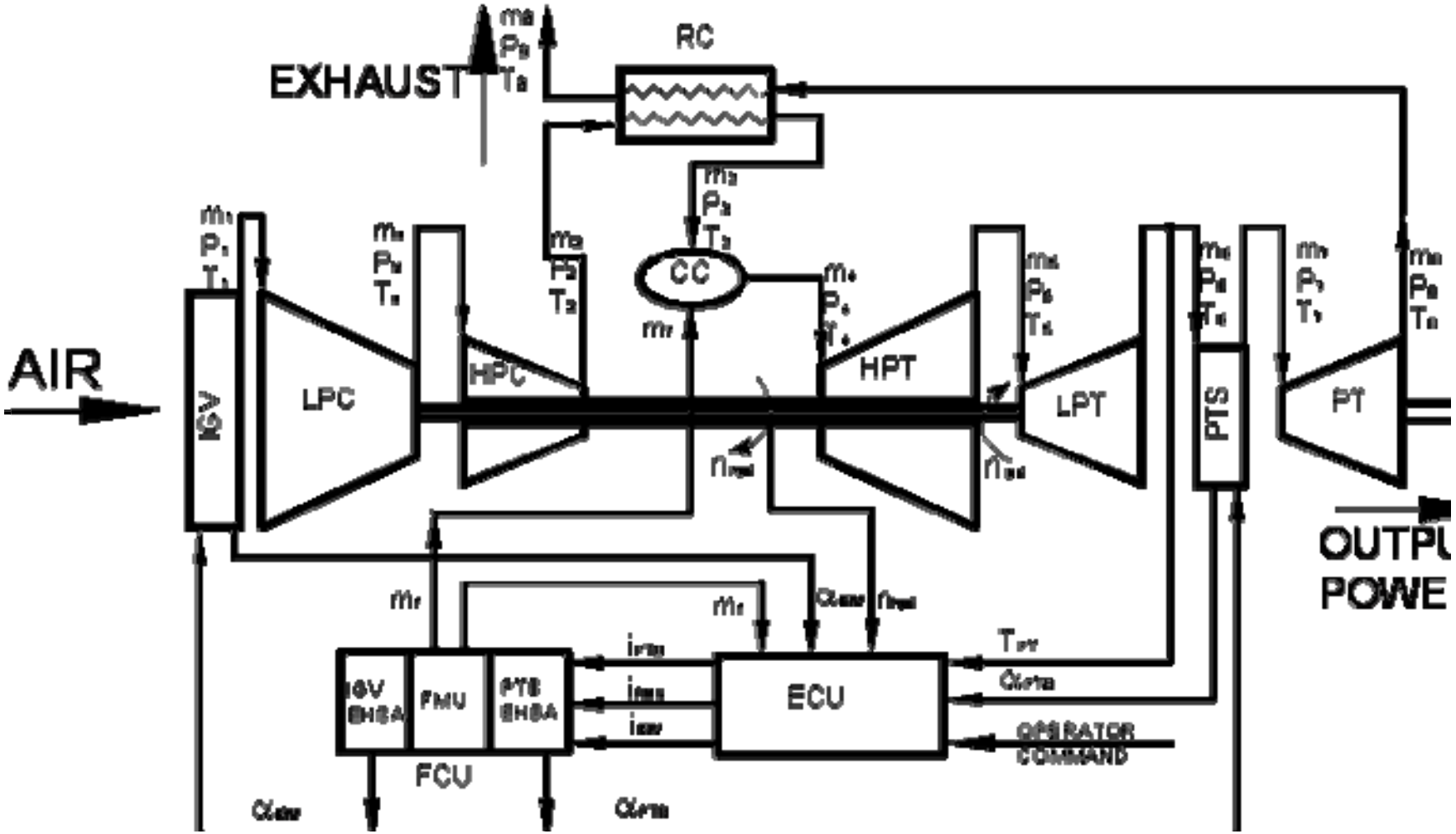

Combustion chamber	i	Controlled current (A)	PTS	Power turbine	3	Combustor inlet
Engine electronic control unit	IGV	Inlet guide vanes	RC	Recuperator	4	High pres. turbine inlet
Electrohydraulic servo actuator	LPC	Low pressure	T	Temperature, (k)	5	Low pres. turbine inlet
Fuel control unit	LPT	Low pressure turbine	ñ	Angle, (deg.)	6	Power turbine stator
Fuel metering unit	m	Mass flow rate, (Kg/s)	1	Low press. com.	7	Power turbine inlet
High pressure compressor	n	Speed, (r.p.m)	x	High press. com.	8	Power turbine outlet
High pressure turbine	P	Pressure, (pa)	2	High press. com.	9	exhaust

Fig. (1) Block diagram of the studied gas turbine engine

CC
ECU
EHSA
FCU
FMU
HPC
HPT

3.1 Low pressure compressor (LPC)

LPT drives LPC by the interconnection shaft. The LPC receives the guided air from the IGV and increase its energy. The ideal enthalpy difference (Δh) across one stage and the enthalpy loss across the stage can be calculated, Euler's equation, [6]:

$$\Delta h_{os,ideal} = (u_2 c_{u2} - u_1 c_{u1}) \quad (1)$$

$$\Delta h_{losses} = \Delta h_i + \Delta h_f \quad (2)$$

Where the incidence loss (Δhi) can be calculated by:

$$\Delta h_i = \Delta h_{i,rotor} + \Delta h_{i,stator} \quad (3)$$

Where the rotor and stator incidence losses are calculated using the formulas [2]:

$$\Delta h_{i,rotor} = 0.5\left[U_1 - \frac{\dot{m}\cot\beta_1}{\rho_{o1}A_1}\right] \quad \text{and} \quad \Delta h_{i,stator} = 0.5\left[\sigma U_1 - \frac{\dot{m}\cot\alpha_2}{\rho_{o1}A_1}\right] \quad (4)$$

The friction loss across a single stage of the compressor is given by the following:

$$\Delta h_f = \frac{C_h L \dot{m}^2}{2D\rho_{o1}^2 A_1^2 \sin^2\beta_1} \quad (5)$$

Thus, the total enthalpy difference across the compressor stage is calculated by:

$$\Delta h_{os} = \Delta h_{os,ideal} - \Delta h_{losses} \quad (6)$$

The following equation is for the compressor pressure rise (π_{lpc}) in N number of stages with similar enthalpy rise.

$$\pi_{lpc} = \left[\frac{N\eta_s \lambda \Delta h_{os}}{c_p T_{o1}} + 1\right]^{\frac{\gamma}{\gamma-1}} \quad (7)$$

Equations from (1) to (7) show that the pressure rise across the LPC is highly affected by the air flow rate, the compressor speed and geometry.

The work done (W) and the temperature rise (T) through the LPC can be predicted as follows, [2]:

$$W_{lpc} = T_{o1} * c_p \frac{\left[\left(\pi_{lpc}\right)^{\frac{\gamma-1}{\gamma}} - 1\right]}{\eta_{lpc}} \quad (8)$$

$$T_x = T_{o1} + \frac{W_{lpc}}{c_p} \quad (9)$$

3.2 High pressure compressor (HPC)

HPT drives HPC by the interconnection shaft. The HPC receives the compressed air from the LPC and increase its energy. So, the pressure rise (π_{hpc}) across the axial and radial HPC can be predicted, [2]:

$$\pi_{hpca} = \left[\frac{N\eta_s \lambda \Delta h_{os}}{c_p T_x} + 1\right]^{\frac{\gamma}{\gamma-1}} \quad (10)$$

$$\pi_{hpcr} = \left[\frac{\eta_s \Delta h_{os}}{c_p T_{2a}} + 1 \right]^{\frac{\gamma}{\gamma-1}} \quad (11)$$

The work and the temperature rise through the axial HPC can be predicted by:

$$W_{hpca} = T_x * c_p \frac{\left[\left(\pi_{hpca} \right)^{\frac{\gamma-1}{\gamma}} - 1 \right]}{\eta_{hpca}} \quad (12)$$

$$T_{2a} = T_x + \frac{W_{hpca}}{c_p} \quad (13)$$

The work done and the temperature rise through the radial HPC and can be predicted as follows:

$$W_{hpcr} = T_{2a} * c_p \frac{\left[\left(\pi_{hpcr} \right)^{\frac{\gamma-1}{\gamma}} - 1 \right]}{\eta_{hpcr}} \quad (14)$$

$$T_2 = T_{2a} + \frac{W_{hpcr}}{c_p} \quad (15)$$

3.3 Combustion chamber (CC)

The compressed air from compression system and the injected metered fuel mix and burn in the combustion chamber. The heat added to the CC depends on the amount of fuel flow rate and the heating value of the fuel.

$$Q_{add} = \dot{m}_f * H_u \quad (16)$$

The CC outlet temperature can be calculated as follows:

$$T_4 = T_3 + \frac{Q_{add} \eta_{cc}}{\dot{m}_g c_{pg}} \quad (17)$$

The pressure at the RC cold side and at the CC outlet can be calculated as follows:

$$P_3 = P_2 * \sigma_{rc} \quad (18)$$

$$P_4 = P_3 * \sigma_{cc} \quad (19)$$

3.4 Turbines section

HPT and LPC are used to drive the HPC (axial and radial) and LPC respectively through connecting shafts. Thus, the work done produced by the turbines can be predicted, [1] and [2]:

$$W_{hpt} = \frac{W_{hpca} + W_{hpcr}}{\eta_m} \quad (20)$$

$$W_{lpt} = \frac{W_{lpc}}{\eta_m} \quad (21)$$

Then the temperature drop across the HPT and the LPT can be calculated by:

$$T_5 = T_4 - \frac{W_{hpt}}{C_{pg}} \quad (22)$$

$$T_6 = T_5 - \frac{W_{lpt}}{C_{pg}} \tag{23}$$

So, the expansion pressure gradient across the HPT and LPT can be calculated by:

$$\pi_{hpt} = \left[1 - \frac{W_{hpt}}{\eta_{hpt} T_4 C_{pg}}\right]^{\frac{\gamma_g}{1-\gamma_g}} \tag{24}$$

$$\pi_{lpt} = \left[1 - \frac{W_{lpt}}{\eta_{hpt} T_5 C_{pg}}\right]^{\frac{\gamma_g}{1-\gamma_g}} \tag{25}$$

The response of engine components speed can predict from the angular equation of motion of the rotating parts, [2], [3] and [4]:

$$G_{hpt} - G_{hpc} = j\dot{\omega}_{hpt} + f\omega_{hpt} \tag{26}$$

$$G_{hpt} - G_{hpc} = \frac{\dot{m}_g}{\omega_{hpt}} W_{hpt} + \frac{\dot{m}_g}{\omega_{hpt}} (W_{hpca} + W_{hpcr}) \tag{27}$$

$$G_{lpt} - G_{hpc} = j\dot{\omega}_{lpt} + f\omega_{lpt} \tag{28}$$

$$G_{lpt} - G_{lpc} = \frac{\dot{m}_g}{\omega_{lpt}} W_{lpt} + \frac{\dot{m}_g}{\omega_{hpt}} W_{lpc} \tag{29}$$

3.6 Power turbine (PT)

Engine output power is generated in the PT by the effect of the high energy gases pass through the PT cascade. The pressure drop in the PT is calculated by:

$$P_8 = P_9 / \sigma_{rh} \tag{30}$$

Thus, the pressure drop across the turbine section and across the PT can be calculated from Eqs. (19) and (30).

$$\pi_{tt} = P_4 / P_8 \tag{31}$$

$$\pi_{pt} = \frac{\pi_{tt}}{\pi_{lpc} * \pi_{hpt}} \tag{32}$$

Assume that there is no temperature drop across the PTS (T_7=T_6). Thus, the PT work can be calculated by the following equation:

$$W_{pt} = T_7 C_{pg} (1 - \pi_{pt})^{(1-\gamma_g)/\gamma_g} \eta_{pt} \tag{33}$$

From Eqs. (23) and (33) the outlet temperature from the PT and at The RC hot side can be predicted:

$$T_8 = T_7 - \frac{W_{pt}}{C_{pg}} \tag{34}$$

$$T_9 = T_8 - (T_3 - T_2) - \frac{C_p}{C_{pg}} \tag{35}$$

3.7 Output shaft power

Output shaft connects the PT to the RGB. The engine specific output shaft power can be calculated from the work done by the power turbine and the gases passes through.

$$P_{pt} = W_{pt}\dot{m}_g \quad (36)$$

From Eqs (19) and (41) the engine efficiency can be calculated

$$\eta_{th} = \frac{P_{pt}}{Q_{add}} \quad (37)$$

3.8 Simulation results

MATLAB and SIMULINK programs are used to simulate the dynamic performance of the studied engine parts from Eq. (1) to (37). Figures (2) and (3) are an example of the simulation results. They show the steady state simulation results for the pressure ratio of the HP compressor and the engine output shaft power at different air to fuel ratio. This simulation results is for the studied engine with the maximum turbine inlet temperature (2200^{o}K) (manufacturer given) and for constant engine rotors speed.

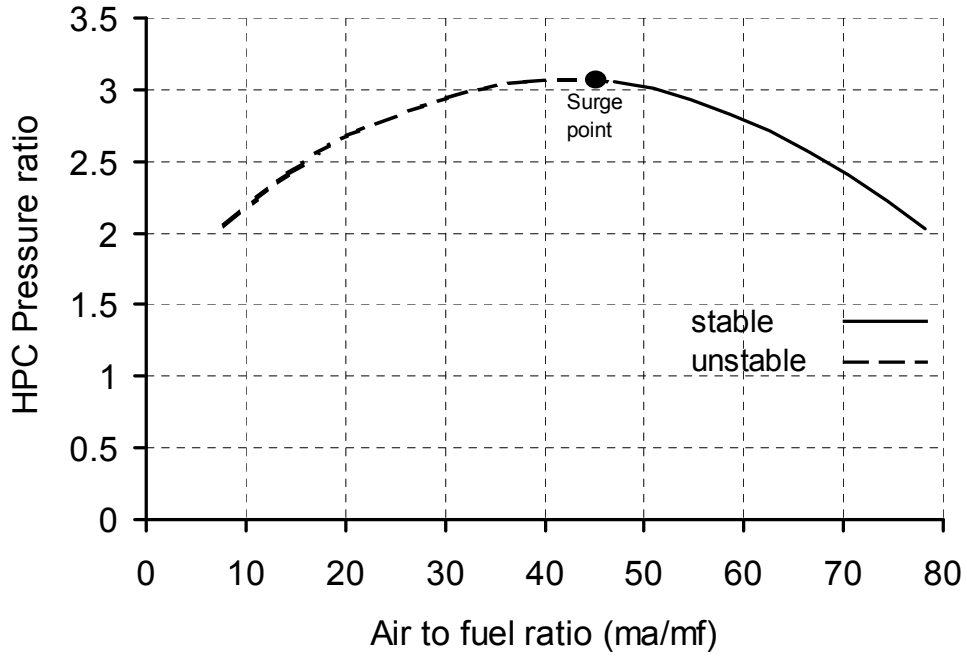

Fig. (2) Steady state simulation result for the engine high pressure compressor at different air to fuel ratio with engine max. turbine inlet temperature=2200^{o}K and constant rotor speed=44500r.p.m

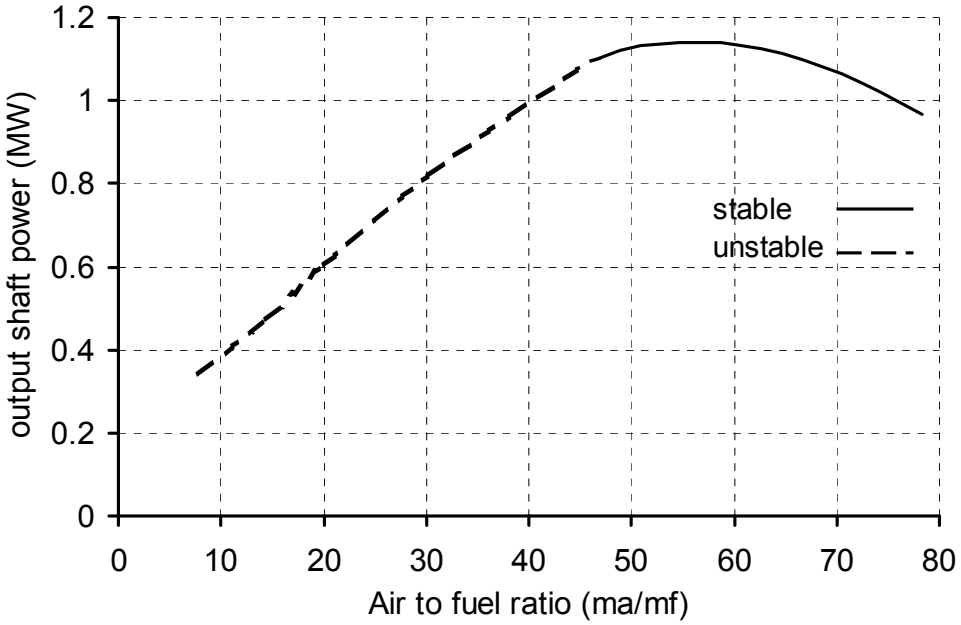

Fig. (3) Steady state simulation result for the engine output shaft power at different air to fuel ratio with engine max. turbine inlet temperature=2200^{o}K.

4. Fuel flow control

The studied gas turbine engine fuel flow control consists of the following, Fig. (4):
Fixed displacement pump
Differential Pressure Regulator Valve (DPRV).
Step controlled solenoid.
Hydraulic amplifier.
Pressure regulator.
Metering unit.
Linear variable differential transformer (LVDT).

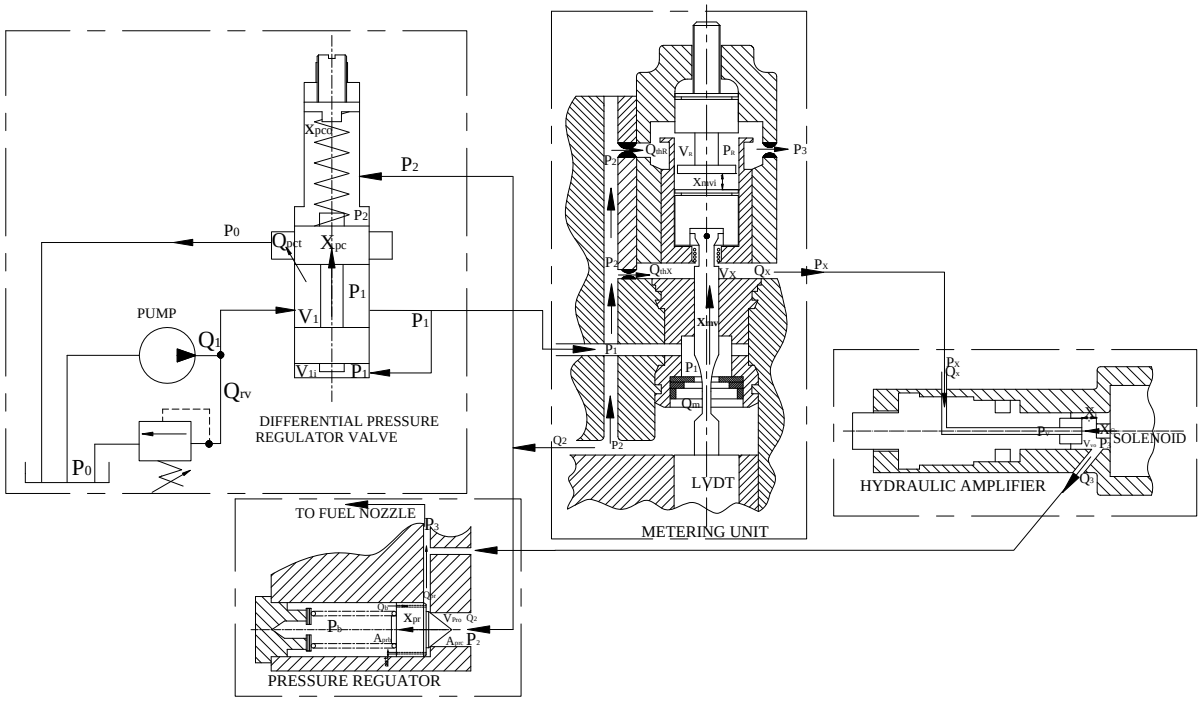

Fig (4) Fuel flow control system of the studied engine

The fuel pump is driven by the HPT shaft through the AGB. The differential pressure regulator valve, (pressure compensator), maintains a constant pressure difference (p_1-p_2) across the metering unit orifice. The step controlled solenoid and the hydraulic amplifier works together to convert the electrical signal into a high pressure hydraulic signal. It controls the position of the metering unit servo piston and the flow orifice area. The pressure regulator maintains a constant reference pressure (p_2). The displacement of the metering unit spool is picked up by the LVDT and feedback to the ECU.
Neglecting the losses through fuel control system passages, effect of jet action and clearance losses. The following is the mathematical model describing the fuel flow controller.

4.1 Differential pressure regulator valve (DPRV)

This valve is indented to maintain constant pressure difference (p_1-p_2) across the fuel metering orifice. Its transient response should be fast enough to keep this pressure difference constant irrespective to the pump flow rate and load pressure variations. The pump flow rate can be described by the following flow equation:

$$Q_1 = V_g n - \frac{p_1}{R_L} \tag{38}$$

The flow rates through DPRV restrictions are:

$$Q_{pct} = C_d A_{pc}(x_{pc}) \sqrt{\frac{2(p_1 - p_o)}{\rho}} \tag{39}$$

$$A_{pc}(x_{pc}) = \pi d_{pc} x_{pc} \tag{40}$$

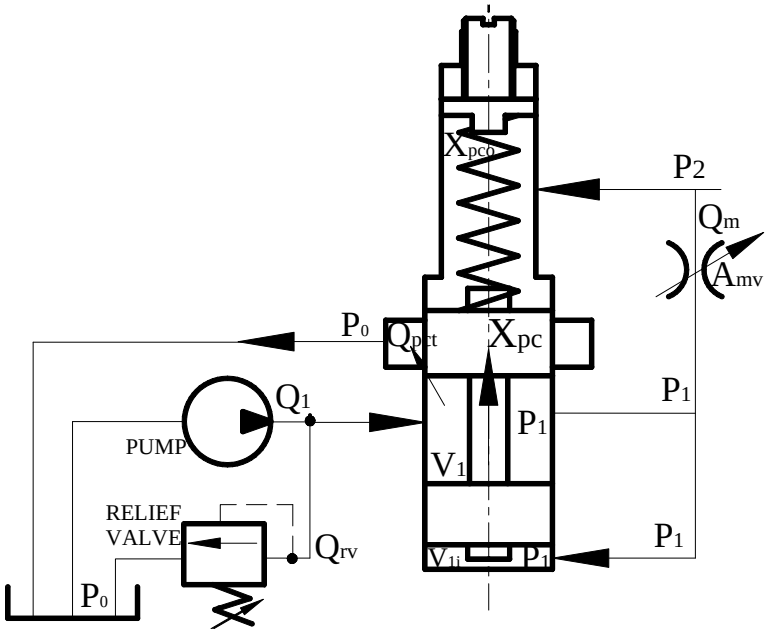

Fig (5) DPRV used with the studied engine fuel flow control system.

The metered fuel flow rate:

$$Q_m = C_d A_{mv} \sqrt{\frac{2(p_1 - p_2)}{\rho}} \tag{41}$$

The DPRV is of overlapping spool type. Thus, the application of the continuity equation to the pump exit chamber yields:

$$\begin{aligned} -Q_{rv} + Q_1 - Q_m - Q_{pct} - A_{spc}\frac{dx_{pc}}{dt} &= \frac{V_{1i} + A_{spc}x_{pc}}{B}\frac{dp_1}{dt} \quad \text{for} \quad x_{pc} > 0 \\ -Q_{rv} + Q_1 - Q_m &= 0 \quad \text{for} \quad x_{pc} = 0 \end{aligned} \tag{42}$$

The valve spool motion is:

$$(p_1 - p_2)A_{spc} = m_{spc}\frac{d^2x_{pc}}{dt^2} + f_{pc}\frac{d\,x_{pc}}{dt} + k_{pc}(x_{pco} + x_{pc}) \tag{43}$$

4.2 Hydraulic amplifier

The electric command signal is changed into an amplified hydraulic signal by the solenoid and hydraulic amplifier, Figs. (6) and (7). The mathematical model describing the dynamic performance of the hydraulic amplifier and the driving solenoid is deduced the equation of motion of the solenoid core, neglecting the effect of magnetic hysteresis [4], [6].

$$F_c(i) = m_c\frac{d^2x_c}{dt^2} + f_c\frac{dx_c}{dt} + k_c x_c + F_p + F_{seat,c} \tag{44}$$

$$F_p = p_3 * A_c \quad \& \quad A_c = \pi d_c^2 \tag{45}$$

$$F_{saet,c} = \begin{cases} 0 & x_c < x_i \\ f_{seat}\dot{x}_c + k_{seat}\left|x_i - x_c\right| & x_c \geq x_i \end{cases} \tag{46}$$

The flow rate passing through the hydraulic amplifier is written as:

$$Q_x = C_d A_{vo}\sqrt{\frac{2(p_x - p_v)}{\rho}} \tag{47}$$

$$Q_3 = C_d A_{vx}\sqrt{\frac{2(p_v - p_3)}{\rho}} \tag{48}$$

$$A_{vx} = \pi d_v(x_i - x_c) \quad \& \quad A_{vo} = \frac{\pi}{4}d_v^2 \tag{49}$$

The continuity equation in the hydraulic amplifier chamber is as follows, [7] and [8]:

$$Q_x - Q_3 = \frac{V_{vo}}{B}\frac{dp_v}{dt} \tag{50}$$

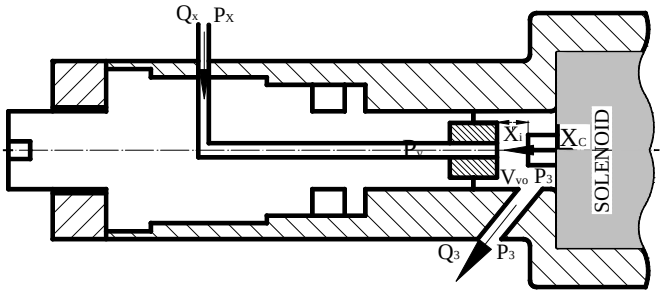

Fig. (6) Hydraulic amplifier

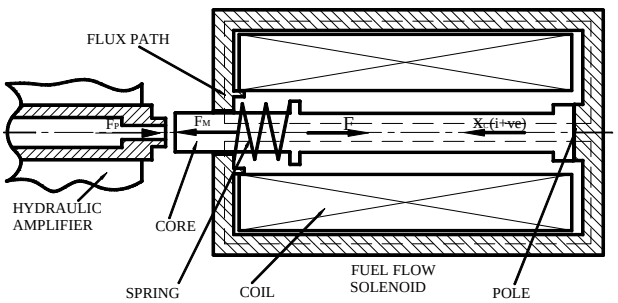

Fig. (7) Fuel flow solenoid

4.3 Pressure regulator

The pressure regulator maintains a constant reference pressure p_2. The pressure regulator dynamic performance is modeled mathematically. The flow rate through the pressure regulator restrictions of the valve spool is given by, [9]:

$$Q_{pr} = C_d A_{pr}(x_{pr})\sqrt{\frac{2(p_2 - p_3)}{\rho}} \tag{51}$$

The geometry of the projected area of the pressure regulator is shown in Fig. (8)

$$h = x_{pr}\sin\alpha$$
$$d_{pp} = d_{pr} - 2x_{pr}\sin\theta\cos\theta \tag{52}$$

$$A_{pr}(x_{pr}) = \begin{cases} 0 & x_{pr} \le 0 \\ \left[d_{pr}x_{pr}\sin\theta - x_{pr}\sin\alpha\cos\theta\right] & x_{pr} > 0 \end{cases} \tag{53}$$

The flow rate through the damped holes is given by:

$$Q_b = C_{d,st}A_{st}\sqrt{\frac{2(p_b - p_3)}{\rho}} \tag{54}$$

The pressures P_2 and P_b are obtained by applying the continuity equations for the pressure regulator as [12]:

$$Q_2 - Q_{pr} - A_{pr}\frac{dx_{pr}}{dt} = \frac{V_{pro} + A_{pr}x_{pr}}{B}\frac{dp_2}{dt} \tag{55}$$

$$A_{prr}\frac{dx_{pr}}{dt} - Q_b - \frac{V_{pro} - A_{prr}x_{pr}}{B}\frac{dp_b}{dt} = 0 \tag{56}$$

The equation of motion of the pressurizing valve poppet is written as:

$$p_2A_{prc} - p_bA_{prr} = m_{pr}\frac{d^2x_{pr}}{dt^2} + f_{pr}\frac{dx_{pr}}{dt} + k_{pr}x_{pr} - F_{seat} \tag{57}$$

$$F_{saet,c} = \begin{cases} 0 & x_{pr} \ge 0 \\ f_{seat}\dfrac{dx_{pr}}{dt} + k_{seat}x_{pr} & x_{pr} < 0 \end{cases} \tag{58}$$

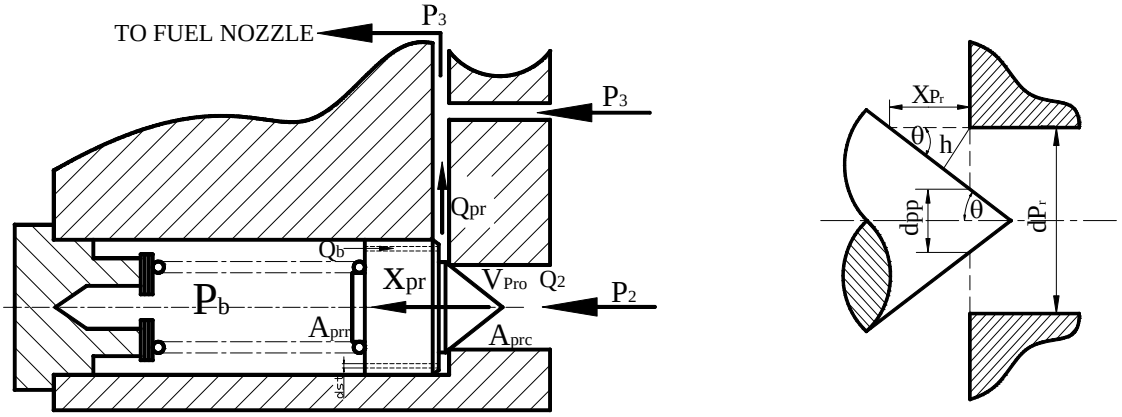

Fig. (8) Pressure regulator and the geometry of the projection area

4.4 Metering unit

Figure (9) shows a fuel metering unit equipped with contoured-double slab metering valve which varied the orifice area to produce a metered area proportional to valve spool travel. The pressure difference (P_1-P_2) across the metering unit orifice is maintained constant by DPRV. This let the metered fuel flow proportional to the orifice area. Equation (41) is used to calculate the metered fuel flow as follows:

$$Q_m = C_d A_{mv}(x_{mv})\sqrt{\frac{2(p_1 - p_2)}{\rho}}$$

$$A_{mv} = \begin{cases} 0 & x_{mv} = 0 \\ \pi(R^2 - r_{mv}^2) & x_{mv} < x_{mv,max} \\ \pi(R^2 - r^2) & x_{mv} \geq x_{mv,max} \end{cases} \quad (59)$$

$$r_{mv} = R - (0.0029x_{mv}^2 + 0.39x_{mv})$$

The orifice flow around the metering valve servo piston is affected by the pressures P_R and P_x which controlled by hydraulic amplifier.

$$Q_{thx} = C_d A_{th}\sqrt{\frac{2(p_2 - p_x)}{\rho}} \quad (60)$$

$$Q_{thR} = C_d A_{th}\sqrt{\frac{2(p_2 - p_R)}{\rho}} \quad (61)$$

$$Q_{th3} = C_d A_{th}\sqrt{\frac{2(p_R - p_3)}{\rho}} \quad (62)$$

$$Q_{Ro} = C_d A_{tho}\sqrt{\frac{2(p_R - p_o)}{\rho}} \quad \text{and} \quad Q_{Ro}=0 \text{ at normal mode} \quad (63)$$

The continuity equations of the fuel flow through metering unit are as follows:

$$Q_m - Q_{thx} - Q_{thR} - Q_2 = 0 \quad (64)$$

$$Q_{th} - Q_x - A_{mpr}\frac{dx_{mv}}{dt} = \frac{V_{xo} + A_{mpr}x_{mv}}{B}\frac{dp_x}{dt} \quad (65)$$

$$Q_{thR} - Q_{th3} + A_{mpc}\frac{dx_{mv}}{dt} = \frac{V_{Ro} + A_{mpc}x_{mv}}{B}\frac{dp_R}{dt} \quad (66)$$

The effects of pressure difference, geometry and internal properties of the valve on the response of the metering valve spool motion are represented by, [10] and [12]:

$$p_x A_{mpr} - p_R A_{mpc} + (p_1 - p_2)A_{mv} = m_{mv}\frac{d^2x_{mv}}{dt^2} + f_{mv}\frac{dx_{mv}}{dt} + k_{mv}x_{mv} + F_{seat,max} - F_{seat,min} \quad (67)$$

$$F_{saet,max} = \begin{cases} 0 & x_{mv} < x_{mvi} \\ f_{seat,mv}\frac{dx_{mv}}{dt} + k_{seat,mv}\left|x_{mvi} - x_{mv}\right| & x_{mv} \geq x_{mvi} \end{cases} \quad (68)$$

$$F_{saet,max} = \begin{cases} 0 & x_{mv} \geq 0 \\ f_{seat,mv}\frac{dx_{mv}}{dt} + k_{seat,mv}\left|x_{mv}\right| & x_{mv} < 0 \end{cases} \quad (69)$$

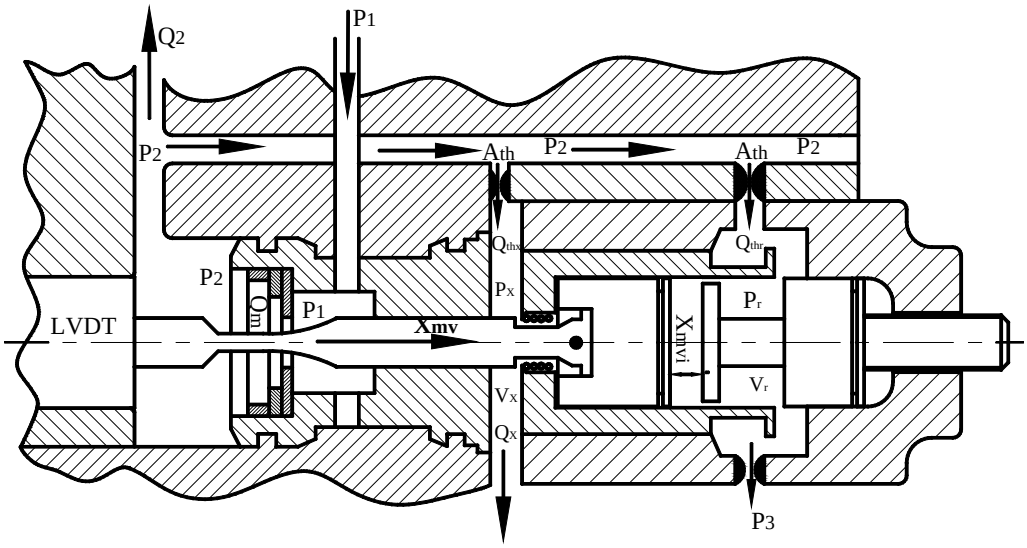

Fig. (9) Engine fuel flow control metering unit.

4.5 Feed back system

LVDT is the feedback device to the ECU about the engine fuel flow rate, [9] and[13]:

$$i_e = i - i_b \qquad (70)$$

$$i_b = k_b * x_m$$

4.6 Simulation results

The deduced mathematical relations are used to develop a computer simulation program for the studied fuel flow controller by the SIMULINK program. Figure (10) shows a sample of the simulation results. It shows the response of the fuel flow rate to a step increase of the control current from 0 to 0.4 A. The response shows a considerable percentage overshoot of about 2 ms duration.

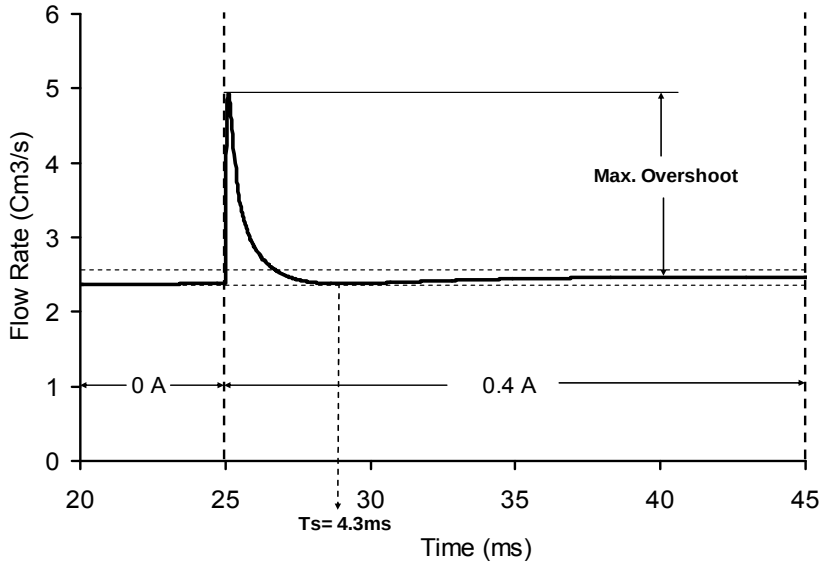

Fig. (10) Mathematical model simulation results of the response of the metering unit flow rate due to step increase of the solenoid supplied current from 0 to 0.4 A.

5. Air flow control

The engine intake air is controlled by a contactless controlled spool electrohydraulic servo actuator, Fig. (11). Construction and operation of the studied EHSA was introduced [5].

Figure (12) shows the velocity triangle of the IGV which guides and controls the engine intake air flow. The engine intake air mass flow rate depends on two parameters; angle of inlet guide vanes controlled by IGV-EHSA and LPC speed.

$$\dot{m}_a = \frac{\omega_{LPC} r_{lpc,1} \rho A_{lpc}}{\cot\alpha_1 + \cot\beta_1} \tag{71}$$

5.1 Mathematical model of air flow control EHSA

The mathematical model describes the air flow control EHSA was introduced in detail in the previous work [5]. The IGV angle depends on the EHSA displacement (y_{EHSA}).

$$p_B A_B - p_A A_A + F_L = m_p \frac{d^2 y_{EHSA}}{dt^2} + f_p \frac{dx_{EHSA}}{dt} + F_{Aseat} \tag{72}$$

$$F_{saet,max} = \begin{cases} f_{Aseat} \dfrac{dy_{EHSA}}{dt} + k_{Aseat} \left| y_{EHSA} - y_{EHSA,max} \right| & y_{EHSA} \geq y_{EHSA,max} \\ 0 & y_{EHSA,min} < y_{EHSA} < y_{EHSA,max} \\ f_{Aseat} \dfrac{dy_{EHSA}}{dt} + k_{Aseat} \left| y_{EHSA} - y_{EHSA,min} \right| & y_{EHSA} \leq y_{EHSA,min} \end{cases} \tag{73}$$

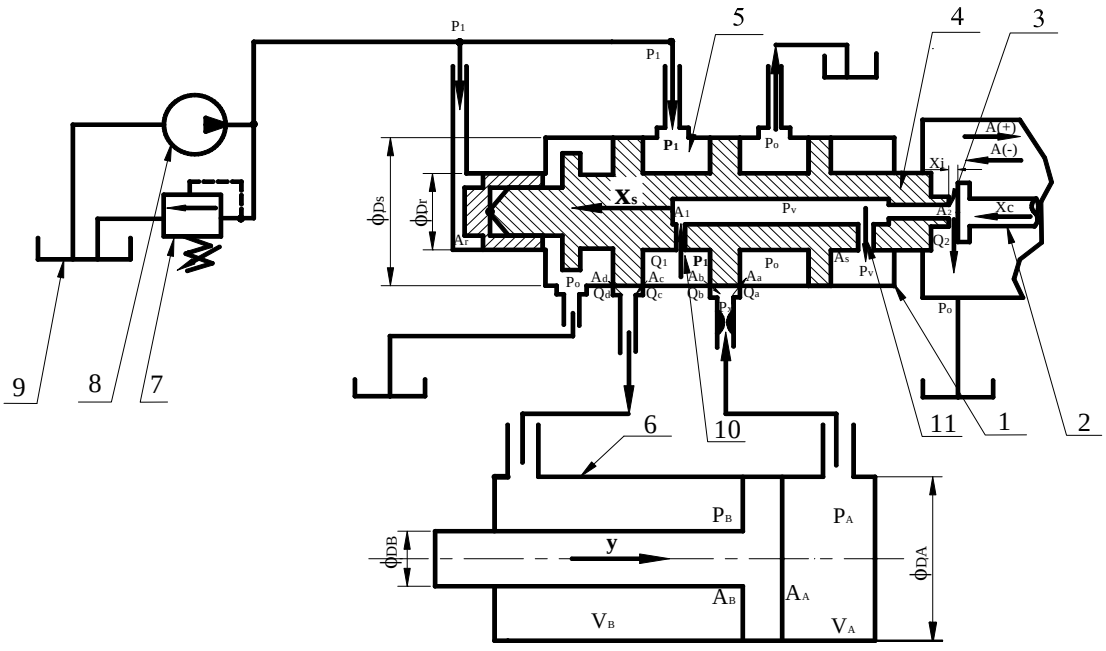

1- Directional control valve
2- Stroke
3-Hydraulic amplifier
4- Directional control valve
5- Valve input port.
6- Hydraulic
7- Relief valve.
8- Hydraulic
9- Oil tank.
10-Hydraulic
11- Hydraulic

Fig. (11) Functional scheme of the studied electrohydraulic servo actuator

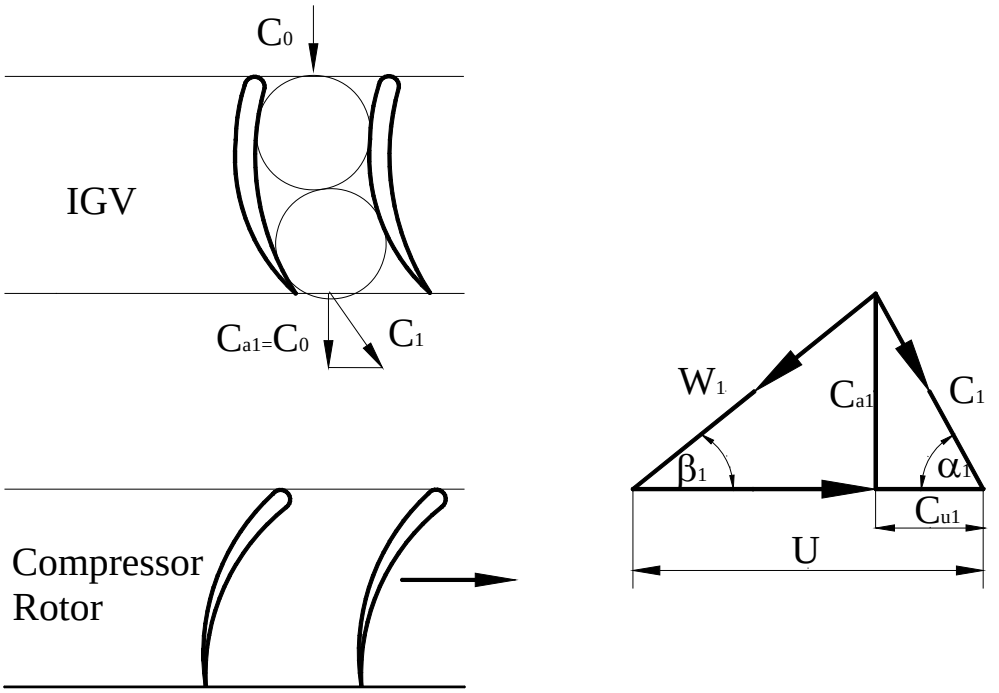

Fig. (12) Engine intake air flow control by IGV.

5.2 Simulation results

The deduced mathematical relations are used to develop a computer simulation program for the studied air flow controller by the SIMULINK program. Figure (13) shows a sample of the simulation results, for open loop control. It shows that the actuator displacement reaches, all the time, the same final steady state position, irrecspect to the magnitude of the input current. The transient speed is max. for zero input current. In this mode, the solenoid core is pushed in the direction of the spool under the action of its spring. The pressure p_v is maximum and the spool moves by its maximum speed under the action of the maximum driving pressure force.

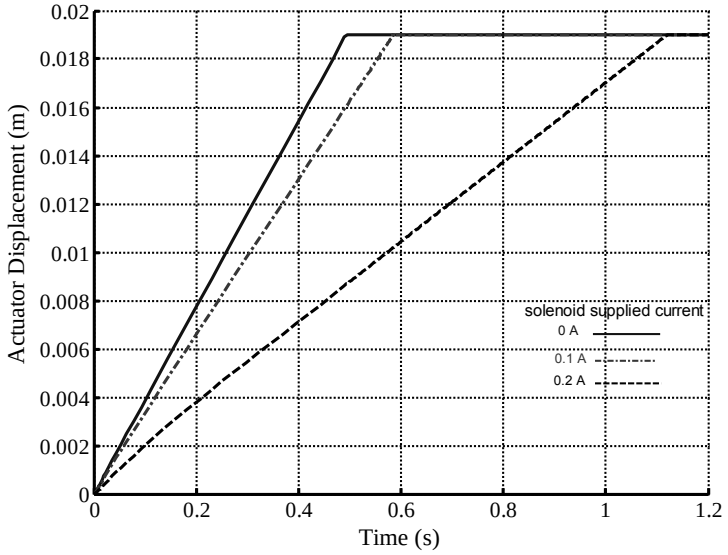

Fig. (13) Simulation transient response of the EHSA for different solenoid input supply current.

5.3 Experimental study

The experimental work, conducted during this study, aims at the validation of the simulation program of the EHSA controlling the guide vanes angle, IGV and PTS. The detailed derivation of the mathematical model and the theoretical performance analysis were previously published [5].

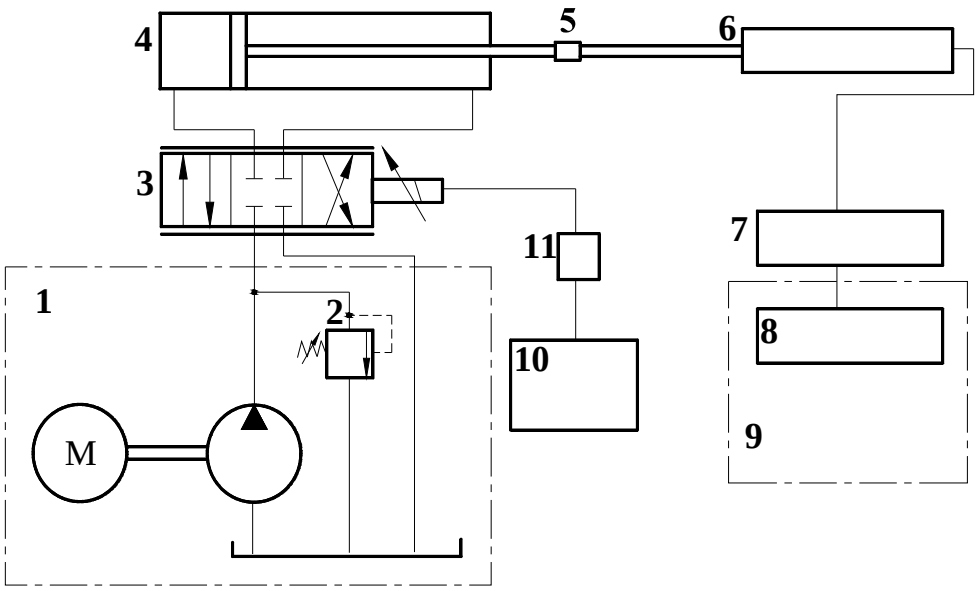

1-	Test stand	2-	Relief valve	3-	EHSV	4-	IGV actuator
5-	Adaptor	6-	LVDT	7-	Front panel	8-	Data acq. card
9-	PC	10-	Power	11	Ammeter		

Fig. (14)Schematic diagram of the hydraulic test rig used to measure the EHSA displacement at different servo solenoid command current

Figures (14) and (15) show the scheme of the test rig and its arrangement. It is used to measure the transient response of the EHSA displacement at different solenoid step input current and input pressure, for open loop arrangement

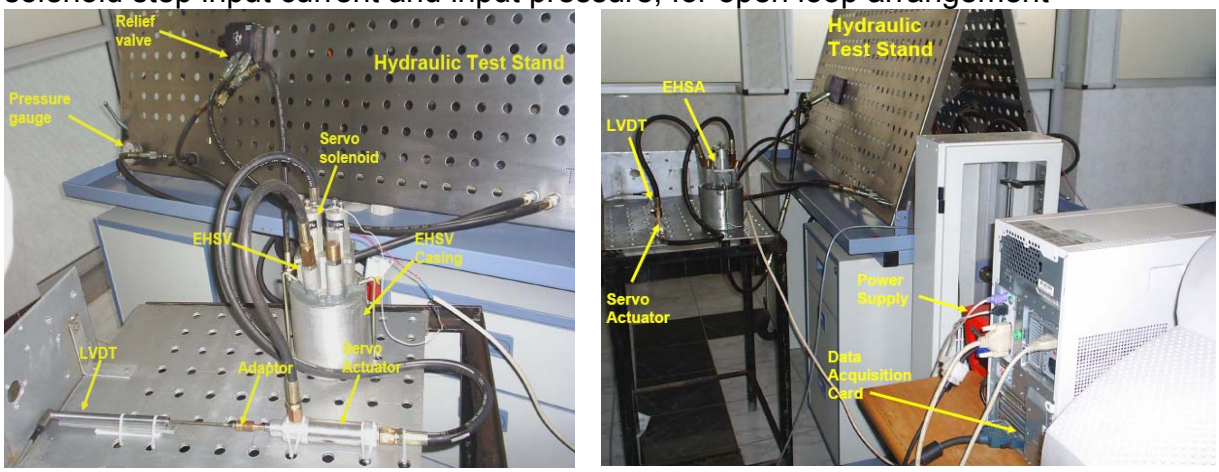

Fig. (15) Hydraulic test rig used to measure the EHSA at different servo solenoid command current.

5.4 Experimental results

The experimental results are plotted in Figs. (16) and (17). Figure (16) shows the transient response of the EHSA displacement to step variation of control current of different magnitudes, for open loop arrangement. This experiment was conducted

keeping the supply pressure p_1 constant. The transient response of the EHSA to step reduction of the input current from 0.3 A to zero A is measured and plotted in Fig. (17) for two different values of the input pressure; p_1= 15 and 37 bar.

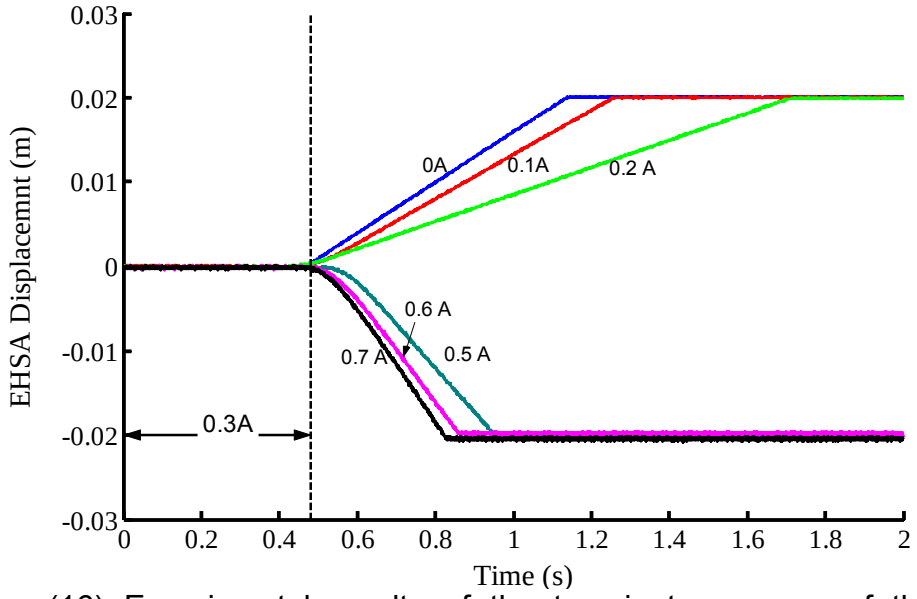

Fig. (16) Experimental results of the transient response of the EHSA piston displacement at step currents of different magnitudes with p_1=37 bar in open loop arrangements.

The study of Fig. (16) shows that :
The transient response speed decreases with the reduction of the net current communicated to the solenoid. Consequently, the settling time decreases for solenoid currents much greater or much smaller than the value of the null position current (0.3 A)
The transient response speed is minimal for solenoid current near to the null position current (0.3 A).

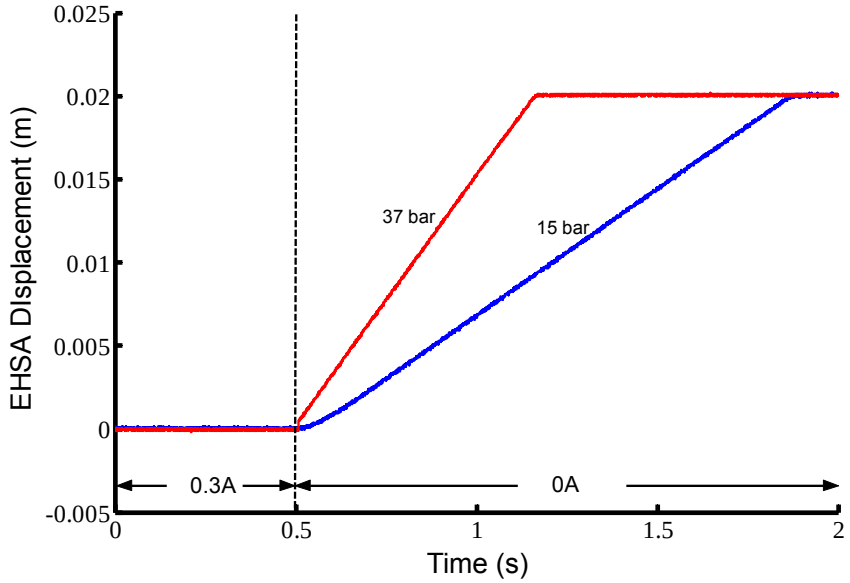

Fig. (17) Experimental results of the transient response of the EHSA piston displacement at step current with different pressure (p_1=37 bar and 15 bar) in open

loop arrangements.

Figure (17) shows the EHSA transient responses at constant solenoid step input current and different circuit pressures and the following can be observed:
The null position is the spool position corresponding to a solenoid current of 0.3 A. This position is not affected by the variation of the supply pressure p_1.
The spool is driven mainly by the pressure forces. Therefore, the reduction of the supply pressure leads to lower transient speed and longer settling time.
The uncertainty on the EHSA displacement measurements depend on the accuracy of the solenoid command current and the supplied pressure. The measurements were repeated (10 times) to be confident with the measuring results. The measurements have standard deviation about (1.08) and repeatability about (2.44) for confidence level (95%).

5.3.4 Validation of the air flow controller simulation program

The validity of the simulation program, previously discussed [5], is evaluated by conducting experimental work and comparing the simulation and experimental results. The transient response of the EHSA displacement to step variation of input current was evaluated experimentally and by the simulation program.
The experiment was conducted for step variation of input current from 0.3 A to 0.1 A, Fig. (18) and from 0.3 A to 0.7 A, Fig. (19).
Figures (18) and (19) carry both the simulation and experimental results. The study of these figures shows good agreement between the simulation and experimental results mainly on the level of the transient speed of actuator.
The observed deviation between experimental and theoretical results is attributed to the adopted simplifying assumptions, mainly:
Constant discharge coefficient through the orifices.
Neglect the effect of jet forces on the valve ports.
Neglect the minor and the major losses through the EHSA system, etc.
The deviation observed from the comparison between the experimental and the theoretical results is from 8% to 16% which is acceptable.

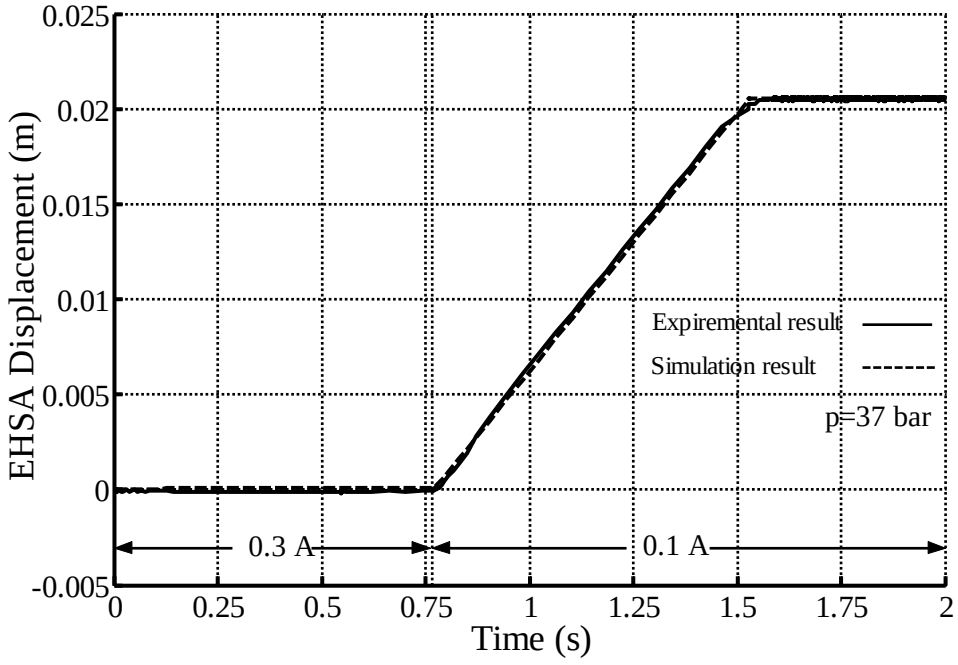

Fig. (18) Comparison between the experimental and Simulation results for the EHSA transient response for step input current (0.1A) and pressure (37 bar).

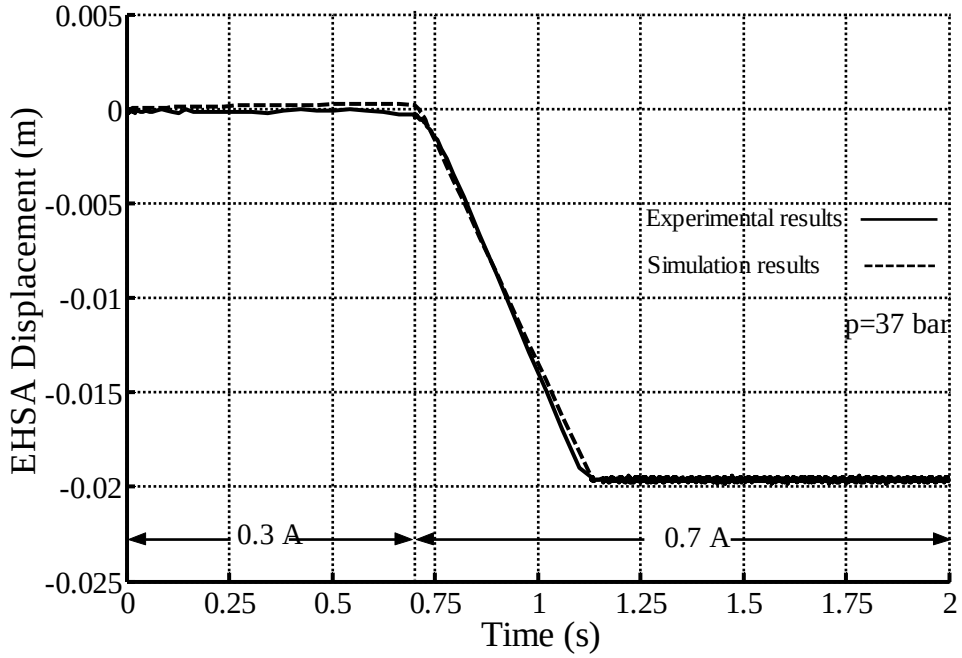

Fig. (19) Comparison between the experimental and simulation results for the EHSA transient response at step input current (0.7A) and pressure (37 bar)

6. Conclusions

The dynamic performance of a heavy duty land system gas turbine engine is investigated in this paper. The studied engine is controlled by means of three electrohydraulic servo actuators, two for the air flow rate and one for the fuel flow rate. The equation describing the basic system subsystems and controllers of the engine were deduced and applied to develop a computer simulation program. The simulation program of the air flow electrohydraulic servo controllers was validated experimentally. The simulation results for the pressure ratio of the HP compressor and for the engine output power, estimated by the simulation programs could be observed reasonable behavior. The investigation of the dynamic performance of the engine as well as the effect of the basic parameters will be included in part II of this paper.

7. References

[1] Rowen W. I., 1983, “Simplified Mathematical Representations of Heavy-Duty Gas Turbine Engine”, Transaction of ASME, Journal of Engineering for Gas Turbine and Power, Vol.105, pp. 865-869.

[2] Crosa G., et. al., 1998, “Heavy-Duty Gas Turbine Plant Aero-thermodynamics Simulation Using Simulink”, Transaction of ASME, Journal of Engineering for Gas Turbine and Power, Vol. 120, pp.550-556.

[3] Kim J. H., et. al., 2001, “Model Development and Simulation of Transient Behavior of Heavy Duty Gas Turbines”, Transaction of ASME, Journal of Engineering for Gas Turbine and Power, Vol. 123, pp. 589-594.

[4] Kim J. H., et. al., 2002, “Dynamic Simulation of Full Startup Procedure of Heavy-Duty Gas Turbines”, Transaction of ASME, Journal of Engineering for Gas Turbine and Power, Vol. 124, pp. 510-516.
[5] M. Metwally, et. al., 2006, "Dynamic Performance of an Electrohydraulic Servo Actuator with Contactless Controlled Spool", 12th International Conference on Applied Mechanics and Mechanical Engineering, MTC, Cairo, Egypt.
[6] Cohen, et. al., 1984, “Gas Turbine Theory”, Longman Group Limited, London.
[7] Arno Schmitt et. al., 1989, "Proportional and Servo Valve Technology", Mannesmann Rexroth Gmbh.
[8] F.D.Norvelle, 2000, "Electrohydraulic Control System", Prentice Hall inc., New jersey, USA.
[9] N.C. Chueng et. al., 1996, "Modelling of a Non Linear Solenoid Towards the Development of a Proportional Actuator", IEEE Industrial Electronic Society annual general, Vol. 2, pp. 21-30.
[10] G. Schoenau, et. al., 1999, "Parameter Estimation in a Solenoid Proportional Valve Using OLS and MLH Techniques", Mechanical Engineering Department of University of Saskatchewan, Canada.
[11] A.C. Lua et. al. 2001, "Proportional assist ventilation system based on proportional solenoid valve control", Journal of Medical Engineering and Physics, Vol. (23), pp. 381–389.
[12] M.G. Rabie, 2005, "Fluid power Engineering", Published by the author, Cairo, Egypt.
[13] M.G. Rabie, 2005, "Automatic Control for Mechanical Engineering Students ", Published by the author, Cairo, Egypt.